

# Constraining Scalar Singlet Dark Matter with CDMS, XENON and DAMA and Prediction for Direct Detection Rates

Abhijit Bandyopadhyay<sup>†</sup>, Sovan Chakraborty<sup>‡</sup>, Ambar Ghosal<sup>‡</sup> and  
Debasish Majumdar<sup>‡</sup>

<sup>†</sup> *Ramakrishna Mission Vivekananda University,  
Belur Math, Howrah 711202, India*

<sup>‡</sup> *Saha Institute of Nuclear Physics,  
1/AF Bidhannagar, Kolkata 700064, India*

PACS numbers: 14.80.Cp, 95.35.+d

## ABSTRACT

We consider a simplest extension of the Standard Model (SM) through the incorporation of a real scalar singlet and an additional discrete  $Z_2$  symmetry. The model admits the neutral scalar singlet to be stable and thus, a viable component of dark matter. We explore the parameter space of the model keeping in view the constraints arise from different dark matter direct detection experiments through WIMP-nucleon scattering. First of all, we have utilised the data obtained from CDMS, XENON-10 and XENON-100 collaborations. We further constraint the parameter space from the DAMA collaboration results (both with and without channelling) and CoGeNT collaboration results. Throughout our analysis, the constraint arises due to the observed relic density of dark matter reported by WMAP experiment, is also incorporated. Utilising all those constraints, on the model parameter space, we calculate the event rates and the annual variation of event rates in the context of a Liquid Argon Detector experiment.

# 1 Introduction

Several cosmological observations like rotation curves of spiral galaxies, the gravitational microlensing, observations on Virgo and Coma clusters [1, 2], bullet clusters [3], etc. provide indications of existence of huge amount of non-luminous matter or dark matter (DM) in the universe. The Wilkinson Microwave Anisotropy Probe (WMAP) experiment [4] suggests that about 85% of the total matter content of the universe is dark. This constitutes 23% of the total content of the universe. The rest 73% is the dark energy, whereas the remaining 4% is the known luminous matter. Nature and identity of the constituents of this non-luminous matter is mostly unknown. However, the indirect evidences suggest that most of them are stable, nonrelativistic (Cold Dark Matter or CDM) and Weakly Interacting Massive Particles (WIMPs) [5, 6, 7, 8]. Despite the wide success spectrum of Standard Model (SM), explanation of CDM poses a challenge to SM as no viable candidate for CDMs has been obtained within the framework of SM. Hence, there are attempts to explain the DM WIMP candidates with theories beyond standard model.

Phenomenology of different extensions of scalar sector of the SM had been explored by many groups [9, 10, 11, 12, 13, 14, 15, 16, 17, 18, 19, 20, 21]. However, addition of one real scalar singlet to the SM provides the simplest possible minimal renormalizable extension to the scalar sector of SM. In addition, invoking a  $Z_2$  discrete symmetry under which the additional singlet is odd, gives rise to the singlet as a viable DM candidate. In this work, we explore the parameter space of the model to accommodate the results of different dark matter direct detection experiments. We further predict the event rates and the annual variation of the event rates to be observed by the Liquid Argon Detector experiment. In the experiments for direct detection of DM, the WIMP scatters off the target nucleus of the material of the detector giving rise to recoil of the nucleus. The energy of this nuclear recoil is very low ( $\sim$  keV). The signal generated by the nuclear recoil is measured for direct detection of dark matter.

There are several ongoing experiments for direct dark matter searches. Some of them are cryogenic detectors where the detector material such as Germanium are kept at a very low temperature background and the nuclear recoil energy is measured using scintillation, phonon or ionization techniques. The experiments like CDMS (Cryogenic Dark Matter Search uses Germanium as detector material) at Soudan Mine, Minnesota [27] use both ionization and phonon techniques. In phonon technique, the energy of the recoil nucleus sets up a vibration of the detector material (Ge crystal for CDMS). These vibrations or phonons propagate at the surface of the detector crystal and excites quasi-particle states at materials used in the pulse pick up device. Finally the heat produced by these quasi-particle states is converted to pulses by SQUID (Superconducting Quantum Interference Device) amplifiers. CDMS carries out two experiments - one with Germanium and the other with Silicon in order to separate the neutron background. As Germanium nucleus is heavier ( $A = 73$ ) than Silicon ( $A = 28$ ), WIMPs interact with  $^{73}\text{Ge}$  with higher probability than with  $^{28}\text{Si}$ , but neutron being strongly interacting will not make any such discrimination. Thus any excess signal at the  $^{73}\text{Ge}$  detector over the  $^{28}\text{Si}$  in CDMS will be a possible signature for dark matter.

The DAMA experiment at Gran Sasso (uses diatomic NaI as the detector material) [28], uses the scintillation technique for detection of the recoil energy. There are other class of liquid or gas (generally noble gases) detectors that measure the recoil energy by the ionization of the

detector gas. The ionization yield is amplified by an avalanche process and the drifting of these charge reaches the top (along z-axis) where they are collected by the electrodes for generating a signal. These types of detectors known as TPC (Time Projection Chamber) are gaining lot of interest in present time for their better effectiveness and resolution in detecting such direct signals of recoil energy from a DM-nucleon scattering. As mentioned, they generally use noble gases such as Xenon, Argon or Fluorine etc. The XENON-10 experiment [29] at Gran Sasso is a liquid Xenon TPC with target mass of 13.7 Kg, whereas its upgraded version, the XENON-100 experiment [30] uses 100 Kg of the target mass. The CoGeNT (Coherent Germanium Neutrino Technology) experiment [31] also uses Ge as detector material and designed to detect dark matter particles with masses less than that to be probed in CDMS. Recently the CoGeNT collaboration has reported an excess of events above the expected background [31]. The experiment ArDM (Argon Dark Matter Experiment) [32] plans to use 1 ton of liquid  $^{39}\text{Ar}$  gas for the TPC. There are other experiments that use other techniques like PICASSO [33] etc. at SNOlab in Canada but here we consider CDMS, DAMA, CoGeNT and Xenon experiments for the present study. We restrict the relevant couplings of the scalar dark matter by using the bounds on dark matter-nucleon scattering cross sections from these three experiments and further, utilising the WMAP experimental data. We predict possible direct detection event rate as well as annual variation of event rate in liquid ArDM experiment for different possible dark matter masses.

The paper is organized as follows. In Section 2 we briefly discuss the model. The CDMS, XENON, CoGeNT and DAMA bounds used to constrain the parameter space of the model is described in Section 3. In Section 4 we present the formalism of Direct detection rate calculations and compute such rates for liquid Ar detector. Section 5 contains summary and conclusions.

## 2 Singlet extended Standard Model : A brief outline

The framework of the simplest scalar sector extension of the SM involving addition of a real scalar singlet field to the SM Lagrangian has been discussed in detail in [24, 25]. In this section we present a brief outline of the model and emphasize on those of its aspects that would be relevant for discussions to follow.

The most general form of the potential appearing in the Lagrangian density for scalar sector of this model is given by <sup>1</sup>

$$\begin{aligned}
 V(H, S) = & \frac{m^2}{2}H^\dagger H + \frac{\lambda}{4}(H^\dagger H)^2 + \frac{\delta_1}{2}H^\dagger HS + \frac{\delta_2}{2}H^\dagger HS^2 \\
 & + \left(\frac{\delta_1 m^2}{2\lambda}\right)S + \frac{\kappa_2}{2}S^2 + \frac{\kappa_3}{3}S^3 + \frac{\kappa_4}{4}S^4
 \end{aligned} \tag{1}$$

where  $H$  is the complex Higgs field (an  $SU(2)$  doublet) and  $S$  is a real scalar gauge singlet that defines our minimal extension to the scalar sector of SM. The singlet  $S$  needs to be stable in order to be considered as a viable dark matter candidate. Stability of  $S$  is achieved within the theoretical framework of the model by assuming the potential to exhibit a  $Z_2$  symmetry  $S \rightarrow -S$ .

---

<sup>1</sup>We used same notations as used in [24, 25].

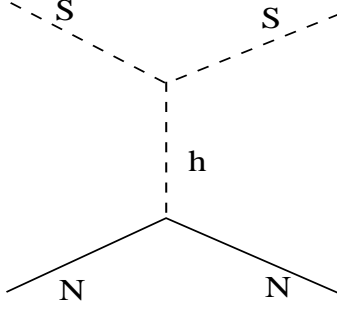


Figure 1: Diagram for singlet-nucleon elastic scattering via higgs mediation

This ensures absence of vertices involving odd number of singlet fields  $S$  ( $\delta_1 = \kappa_3 = 0$ ). Using unitary gauge, we define

$$H = \begin{pmatrix} 0 \\ \frac{v+h}{\sqrt{2}} \end{pmatrix} \quad (2)$$

where  $h$  is the physical Higgs field and  $v = 246$  GeV is the VEV of the  $H$  scalar determined by the parameters  $m$  and  $\lambda$  as  $v = \sqrt{\frac{-2m^2}{\lambda}}$ . The mass terms of the two scalar fields  $h$  and  $S$  are identified as

$$V_{\text{mass}} = \frac{1}{2}(M_h^2 h^2 + M_S^2 S^2) \quad (3)$$

where,

$$\begin{aligned} M_h^2 &= -m^2 = \lambda v^2/2 \\ M_S^2 &= \kappa_2 + \delta_2 v^2/2 \end{aligned} \quad (4)$$

The scalar field  $S$  is stable as long as the  $Z_2$  symmetry is unbroken and appears to be a candidate for cold dark matter in the universe.

In the present work, we investigate the prospect of such a candidate in direct detection experiments through its scattering off nucleon ( $N$ ) relevant for the detector. The lowest order diagram for the process has been shown in Fig. 1. The cross section corresponding to the elastic scattering ( $SN \rightarrow SN$ ) in the non-relativistic limit is given by [11]

$$\sigma_N^{\text{scalar}} = \frac{\delta_2^2 v^2 |\mathcal{A}_N|^2}{4\pi} \left( \frac{m_r^2}{M_S^2 M_h^4} \right) \quad (5)$$

where,  $m_r(N, S) = M_N M_S / (M_N + M_S)$  is the reduced mass for the target nucleus of the two body scattering  $SN \rightarrow SN$  and  $\mathcal{A}_N$  is the relevant matrix element. For the case of non-relativistic nucleons the singlet-nucleus and singlet-nucleon elastic scattering cross sections are related by [11]

$$\sigma_{\text{nucleus}}^{\text{scalar}} = \frac{A^2 m_r^2(\text{nucleus}, S)}{m_r^2(\text{nucleon}, S)} \sigma_{\text{nucleon}}^{\text{scalar}} \quad (6)$$

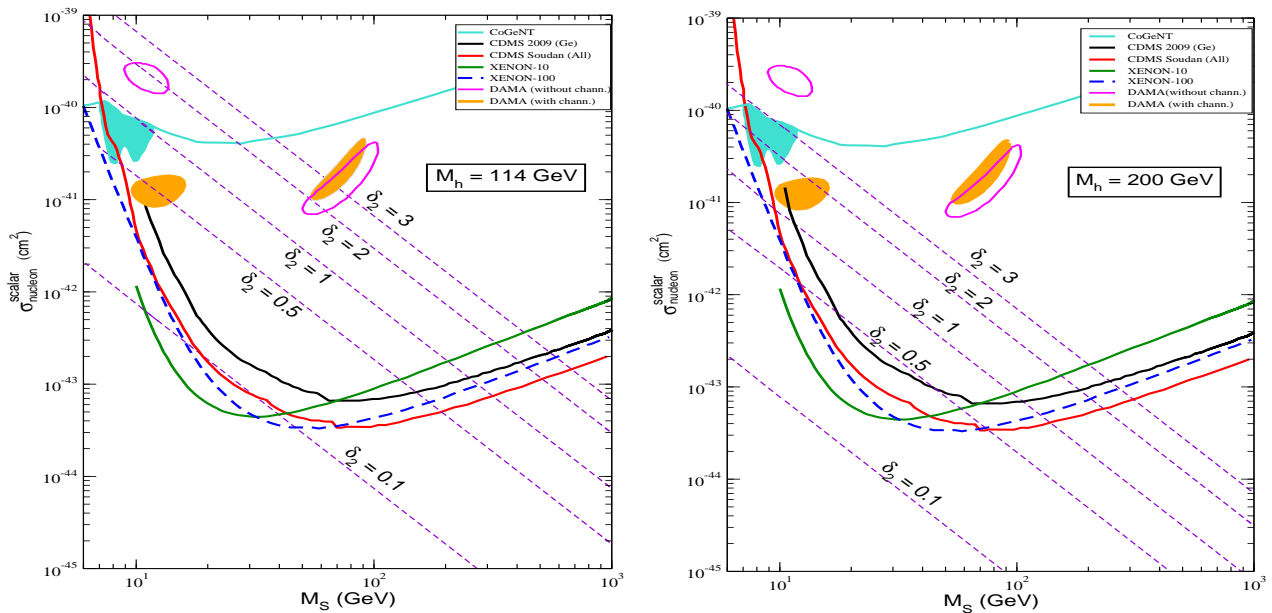


Figure 2: Dashed lines: Scalar singlet-nucleon elastic scattering cross section ( $\sigma_{\text{nucleon}}^{\text{scalar}}$ ) as a function of the singlet mass for different values of  $|\delta_2|$  with 2 different values of higgs mass  $M_h$ , 114 GeV(left panel) and 200 GeV(right panel). Solid lines: 90% C.L. experimental upper limits on  $\sigma_{\text{nucleon}}^{\text{DM}}$  from CDMS 2009 Ge, CDMS Soudan(all), XENON-10 and XENON-100. The shaded areas corresponding to 99% C.L. regions allowed from DAMA (with and without channelling) has also been shown.

Numerically evaluating the matrix element appearing in Eq. (5) the singlet-nucleon elastic scattering cross section can be written as [11]

$$\sigma_{\text{nucleon}}^{\text{scalar}} = (\delta_2)^2 \left( \frac{100 \text{ GeV}}{M_h} \right)^4 \left( \frac{50 \text{ GeV}}{M_S} \right)^2 (5 \times 10^{-42} \text{ cm}^2). \quad (7)$$

It is evident from the above equations that the scalar cross section for scalar singlet depends on two couplings  $\delta_2$  and  $\kappa_2$ . Hence the dark matter direct detection rate with scalar singlet as the dark matter candidate also depends on the two couplings  $\delta_2$  and  $\kappa_2$ . The constraint on direct detection rates of dark matter from different experiments thus can also put constraint on the parameter space ( $\delta_2, \kappa_2$ ) of scalar singlet dark matter. In the next section we will discuss how some of the recent direct detection experiments of dark matter can put limit on the scalar singlet model of dark matter.

### 3 Constraining the model parameters

The direct detection rates of scalar singlet dark matter is governed by the scalar-nucleon cross section ( $\sigma_{\text{nucleon}}^{\text{scalar}}$ ) for a given scalar singlet mass  $M_S$ . Direct detection experiments like CDMS, DAMA, Xenon thus can constraint the scalar singlet parameter space. Preliminary studies of

scalar singlet dark matter concerning CDMS, Xenon are given in Refs. [12, 18, 19]. Also, explanation of DAMA bounds with scalar singlet dark matter is described in [34, 20]. In this work we make a detailed study of all the direct detection bounds together with the relic density limits from WMAP and find the relevant parameter space for the scalar singlet to be a successful dark matter candidate.

### 3.1 Constraints on $\delta_2$ as a function of dark matter mass

The coupling  $\delta_2$  is of severe importance as this is the only coupling in this model which determines the annihilation of the scalar to other standard particles. Moreover given the singlet mass ( $M_S$ ),  $\delta_2$  is the sole coupling that controls the singlet-nucleon cross section and the quadratic dependence (Eq. 7) in particular reflects that this cross section is insensitive to the sign of  $\delta_2$ .

In Fig. 2 the singlet-nucleon elastic scattering cross section is plotted as a function of singlet mass (dark matter mass)  $M_S$  for different values of  $\delta_2$ . The plots are presented at two different values of Higgs mass ( $M_h$ ), namely 114 GeV (left panel) and 200 GeV (right panel) of Fig. 2. For comparison, the 90% C.L. (confidence limit) results obtained from CDMS II experiment (CDMS 2009 (Ge)) [26] are plotted in Fig. 2 with the similar results from the combined analysis of full data set of Soudan CDMS II results (CDMS Soudan (All)) [26], XENON-10 [29] and XENON-100 experiment [30]. One sees from Fig. 2 that the DAMA and CoGeNT results are constrained in closed allowed regions unlike the other experiments that provide upper bounds of the allowed masses and cross-sections of dark matter. In this context it may be noted that the consideration of ion channelling in NaI crystal in DAMA experiment is crucial in the interpretation of its results. The presence of channelling in NaI, affects the allowed mass and cross section regions of the DM particles inferred from the observation of an annual modulation by the DAMA collaboration. The effect of channelling has been discussed extensively in [35]. For our analysis we consider the allowed mass-cross section limits inferred from observed annual modulation of DAMA for both the cases – with channelling and without channelling. From Fig. 2 it is seen that for larger values of  $\delta_2$ , higher singlet mass domain is required in order to represent the experimentally allowed region for  $\sigma_{\text{nucleon}}^{\text{scalar}} - M_S$  plane. Also, the region of overlap of  $\sigma_{\text{nucleon}}^{\text{scalar}} - M_S$  plots for a fixed value of  $\delta_2$ , becomes larger for higher Higgs mass.

In Fig. 3 we present plots for upper limits of the range of  $|\delta_2|$  (as a function of singlet mass) that would reproduce cross section values (computed with Eq. 7) below the 90% CL limits of different experiments shown in Fig. 2. It is evident from the plots that, as in Fig. 2, the allowed values of the coupling  $\delta_2$  is sensitive towards the Higgs mass. Moreover the minimum allowed value of dark matter mass in this model is also dependent on Higgs mass. The appearance of local minima at low  $M_S$  domain of the plots are due to the behaviour of experimental bounds that show a sudden upturn followed by a rise of the curves at low  $M_S$  ( $M_S \rightarrow 0$ ) region. For Higgs mass of 120 GeV (114 GeV) this minima corresponds to the  $|\delta_2|$  value  $\sim 0.5(0.1)$ .

### 3.2 Constraining the $\delta_2 - \kappa_2$ parameter space

In the previous subsection, constraining of the parameter  $\delta_2$  using other direct detection experimental results are addressed. But as described earlier, the present dark matter model with scalar

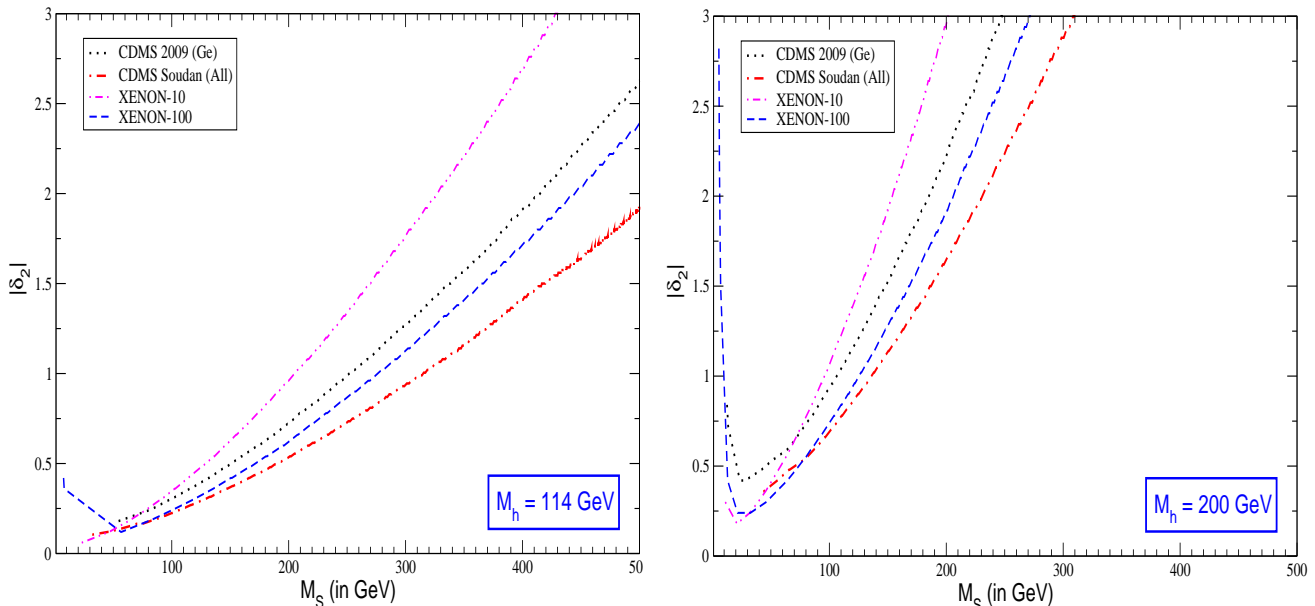


Figure 3: Upper limits on  $|\delta_2|$  as a function of dark matter mass from 90% CL experimental bounds on spin-independent WIMP-nucleon cross section. Plots are done for 2 values of Higgs mass: 114 GeV (left panel) and 200 GeV (right panel) .

singlet also depends on the other parameter namely  $\kappa_2$  (Eq. (4)). From Eq. (4) one sees that the singlet mass term  $M_S$  is governed by two model parameters namely  $\delta_2$  and  $\kappa_2$ . For a given value of  $\delta_2$ , real values of  $M_S$  can be obtained only by excluding all  $\kappa_2$  values less than  $-\delta_2 v^2/2$ . In principle any value of dark matter mass  $M_S$  can accommodate all  $(\delta_2, \kappa_2)$  values satisfying  $\kappa_2 + \delta_2 v^2/2 = M_S^2$ . However at large  $\kappa_2$  values with  $\kappa_2 \gg \delta_2 v^2$ , the singlet mass is predominantly  $\kappa_2$  driven and is scaled with it as  $\sqrt{\kappa_2}$ . The interplay between  $\delta_2$  and  $\kappa_2$  in setting a given singlet mass is represented in Fig. 4 where we plotted (dashed lines) different iso- $M_S$  contours in  $\delta_2 - \text{sign}(\kappa_2)|\kappa_2|^{1/2}$  plane. For a given singlet mass  $M_S$ , the range of  $|\delta_2|$  consistent with CDMS II/XENON-10 limits on WIMP-nucleon scattering cross section (as discussed in Sec. 3.1) would then correspond to a segment of the corresponding iso- $M_S$  contour in  $\delta_2 - \text{sign}(\kappa_2)|\kappa_2|^{1/2}$  plane. Its projection on the  $\kappa_2$  axis would give the corresponding range of the parameter  $\kappa_2$ . In Fig. 4 the shaded regions represent the domains of the model-parameter space  $\delta_2 - \text{sign}(\kappa_2)|\kappa_2|^{1/2}$ , that is consistent with 90% CL limits on WIMP-nucleon elastic scattering cross sections from analysis of CDMS Soudan (All) (left panel), XENON-10 (middle panel) and XENON-100 (right panel) results. The dependence of the allowed model-parameter space on Higgs mass is shown by plotting the allowed areas for three different values of Higgs mass namely 114 GeV, 150 GeV and 200 GeV. The region of the parameter space to the left of  $M_S = 0$  line is excluded as points  $(\delta_2, \kappa_2)$  in that region would give negative values of mass. Moving from lower  $M_S$  to higher  $M_S$  domain in the parameter space allows more and more room for  $(\delta_2, \kappa_2)$  to represent DM-nucleon scattering cross section consistent with its experimental bounds - a feature also apparent from Fig. 2 and Fig. 3 (discussed in Sec. 3.1). At very low scalar singlet mass regime ( $M_S \sim 0 - 10$

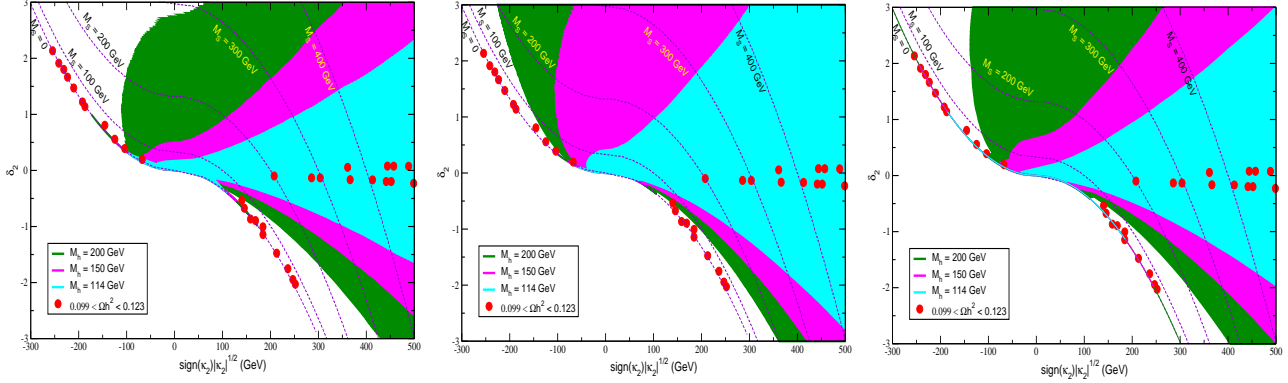


Figure 4: Shaded region: Range of the parameter space  $\delta_2 - \text{sign}(\kappa_2)|\kappa_2|^{1/2}$  consistent with 90% CL limits of WIMP-nucleon scattering cross section from CDMS Soudan (All) (left panel), XENON-10 (middle panel) and XENON-100 (right panel) corresponding to three different values of Higgs mass - 114 GeV, 150 GeV, and 200 GeV. Dashed lines: Different iso- $M_S$  contours in  $\delta_2 - \text{sign}(\kappa_2)|\kappa_2|^{1/2}$  plane. The region spanned by red dots describe the values of model parameters consistent with WMAP measurements of dark matter relic density :  $0.099 < \Omega h^2 < 0.123$ .

GeV) higher peaked value of the WIMP-nucleon scattering cross section-limit concedes a thread like extension of the allowed parameter space along the corresponding iso- $M_S$  contours. The sudden drop of the experimental limits of WIMP-nucleon cross sections in 10 – 20 GeV mass regime severely restricts the width of the above mentioned thread-like extension of the allowed parameter space at  $M_S \sim 0 - 10$  GeV. This drop is more robust for the case of the experiment denoted in this work as “CDMS Soudan (All)” than that of “XENON” experiment leading to a more prominent appearance of the thread-like zone in left panel of Fig. 4. The  $\delta_2 - \kappa_2$  parameter zone obtained from WMAP constraint [24] ( $0.099 < \Omega h^2 < 0.123$ ,  $\Omega$  being the dark matter relic density and  $h$  is the Hubble parameter normalized to  $100 \text{ Km sec}^{-1} \text{ Mpc}^{-1}$ ) are also shown by the red colored dots in Fig. 4, for comparison. From Fig. 4 it is seen that CDMS/XENON upper limits of WIMP-nucleon scattering cross section together with WMAP observation allows only small  $|\delta_2|$  regime ( $\lesssim 0.2$ ) of the model parameter space for different higher values of  $M_S$ , although for very small  $M_S$  values (0 – 10 GeV) CDMS limit concedes more room for  $|\delta_2|$  (upto  $\sim 1.0$ )

The results of DAMA experiment restricts the variations of  $\sigma_{\text{nucleon}}^{\text{scalar}}$  with DM mass in two small contours represented as shaded areas in Fig. 2. They represent the 99% C.L. regions in ( $\sigma_{\text{nucleon}}^{\text{scalar}}$  - DM mass) space. Interpretation of DAMA results with channelling (without channelling) requires WIMP-nucleon scattering cross sections of order  $10^{-41} \text{ cm}^2 (10^{-40} \text{ cm}^2)$  along with two locally preferred zones of dark matter mass - one around  $\sim 12$  GeV (referred as DAMA-a in this work) and the other around  $\sim 70$  GeV (referred as DAMA-b in this work). The DAMA solution corresponding to the large DM mass regime (DAMA-b) is completely excluded by observed limits on the WIMP-nucleon scattering cross section from other direct detection experiments like CDMS, XENON etc. The other DAMA solutions corresponding to lower DM mass regime (DAMA-a) are also largely disfavoured by XENON. However though a small region at the lower



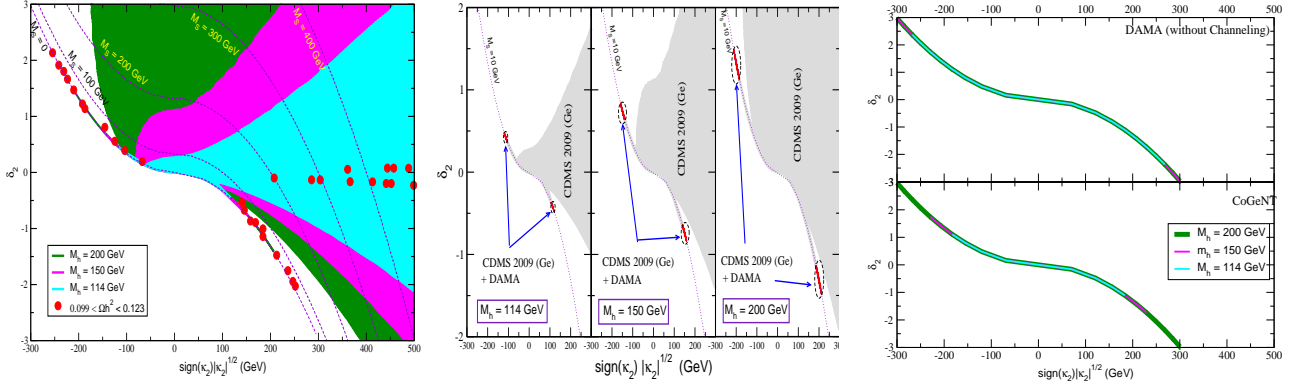


Figure 5: Left panel: (Shaded region) Range of the parameter space  $\delta_2 - \text{sign}(\kappa_2)|\kappa_2|^{1/2}$  consistent with 90% CL limits of WIMP-nucleon scattering cross section from CDMS 2009 (GeV) for three different values of Higgs mass 114 GeV, 150 GeV and 200 GeV. Different iso- $M_S$  contours in  $\delta_2 - \text{sign}(\kappa_2)|\kappa_2|^{1/2}$  plane are shown by dashed lines. The region spanned by red dots describe the values of model parameters consistent with WMAP measurements of dark matter relic density :  $0.099 < \Omega h^2 < 0.123$ . Middle panel: (small thread-like regions outlined by dashed lines) Region in parameter space consistent with (CDMS 2009 Ge + DAMA (with channelling)) limits for  $M_h = 114$  GeV (1<sup>st</sup> column), 150 GeV (2<sup>nd</sup> column), 200 GeV (3<sup>rd</sup> column). The region allowed from only CDMS 2009 (GeV) limits are shaded for corresponding values of Higgs mass. The contour for  $M_S = 10$  GeV are shown by dotted lines. Right panel: Range of the parameter space  $\delta_2 - \text{sign}(\kappa_2)|\kappa_2|^{1/2}$  consistent with 90% CL limits of WIMP-nucleon scattering corresponding to the lower DM mass regime allowed from DAMA (without channelling) (upper panel) and CoGeNT (lower panel) for three different values of Higgs mass 114 GeV, 150 GeV and 200 GeV

DM mass regime (“with channelling” case) in DAMA-a zone is barely consistent with 90% C.L. with CDMS experiment denoted in this work as “CDMS 2009 (GeV)”, the corresponding limit “CDMS Soudan (All)” experiment excludes the entire DAMA-a zone. In the left panel of Fig. 5 we have shown region of  $\delta_2 - \text{sign}(\kappa_2)|\kappa_2|^{1/2}$  parameter space that corresponds to singlet-nucleon elastic scattering cross sections within its 90% C.L. limit from CDMS 2009 (GeV). The middle panel of Fig. 5 shows the  $\delta_2 - \text{sign}(\kappa_2)|\kappa_2|^{1/2}$  parameter space, consistent with both CDMS 2009 (GeV) and DAMA results (with channelling). The small thread like regions (marked red and indicated within closed dashed lines) in the middle panel of Fig. 5 represent the parameter space domain that fits singlet-nucleon scattering cross section with DM-nucleon cross section consistent with both CDMS 2009 (GeV) and DAMA limits (with channelling). These are presented in three different columns that correspond to three values of Higgs mass namely 114 GeV, 150 GeV and 200 GeV. The parameter space consistent with CDMS 2009 (GeV) limit only for corresponding values of Higgs masses are also shown in the respective columns by grey shades. The iso- $M_S$  contour for  $M_S = 10$  GeV, spanning through the DAMA + CDMS 2009 (GeV) allowed regimes, is also shown in each column of the same figure to illustrate the fact that parameter space regions consistent with both DAMA and CDMS 2009 (GeV) correspond to a singlet dark matter mass of around  $\sim 10$  GeV. In the right panel of Fig. 5 we have shown the allowed region in the

$\delta_2 - \text{sign}(\kappa_2)|\kappa_2|^{1/2}$  parameter space consistent with DAMA-a region without channelling (upper panel) and the CoGeNT result (the lower panel).

## 4 Predictions for Rates at Argon detector

The Argon detector is a Noble liquid detector where the liquefied noble gas Argon is used as targets for direct detection of WIMPs. Because of the high density and high atomic number the event rate is expected to be large. Also because of its high scintillation and ionization yields owing to its low ionization potentials, it can effectively discriminate nuclear recoils and other backgrounds from  $\gamma$  or electrons. The ArDM (Argon Dark Matter) experiment at surface of CERN uses one such detector that envisages one ton of liquid Argon in a cylindrical container. This has a provision for three dimensional imaging for every event. A strong electric field along the axis of the cylinder helps drifting of the charge – produced due to the ionization of liquid Argon by WIMP induced nuclear recoil – to the surface of the liquid. This charge then enters into the gaseous phase of the detector (TPC) where it is multiplied through avalanche and finally recorded by a position sensitive readout.

In this section we estimate WIMP signal rates for such Argon detector. The differential rate for dark matter scattering detected per unit detector mass can be written as

$$\frac{dR}{d|\mathbf{q}|^2} = N_T \Phi \frac{d\sigma}{d|\mathbf{q}|^2} \int f(v) dv \quad (8)$$

where  $N_T$  is number of target nuclei per unit mass of the detector,  $\Phi$  is the dark matter flux,  $f(v)$  denotes the distribution of dark matter velocity  $v$  (in earth's frame). The integration is over all possible kinematic configurations in the scattering process.  $|\mathbf{q}|$  is the momentum transferred to the nucleus in dark matter-nucleus scattering and  $\sigma$  being the corresponding cross section. The recoil energy of the scattered nucleus can be expressed in terms of the momentum transfer  $|\mathbf{q}|$  as

$$E_R = |\mathbf{q}|^2/2M_N = m_r^2 v^2 (1 - \cos \theta)/M_N \quad (9)$$

where  $M_N$  is the nuclear mass,  $\theta$  is the scattering angle in dark matter - nucleus center of momentum frame and  $m_r$  is the reduced mass given by

$$m_r = \frac{M_N M_S}{M_N + M_S} . \quad (10)$$

In the above  $M_S$  is the dark matter mass. Expressing the dark matter flux  $\Phi$  in terms of the local dark matter density  $\rho_s$ , velocity  $v$  and mass  $M_S$ . With  $N_T = 1/M_N$  and writing  $|\mathbf{q}|^2$  in terms of nuclear recoil energy  $E_R$ , Eq. (8) can be rewritten as

$$\frac{dR}{dE_R} = 2 \frac{\rho_s}{M_S} \frac{d\sigma}{d|\mathbf{q}|^2} \int_{v_{min}}^{\infty} v f(v) dv \quad (11)$$

where

$$v_{\min} = \left[ \frac{M_N E_R}{2m_{\text{r}}^2} \right]^{1/2} \quad (12)$$

The dark matter - nucleus differential cross-section for the scalar interaction is given by [5]

$$\frac{d\sigma}{d|\mathbf{q}|^2} = \frac{\sigma^{\text{scalar}}}{4m_{\text{red}}^2 v^2} F^2(E_R) . \quad (13)$$

Here  $\sigma^{\text{scalar}}$  is dark matter-nucleus scalar cross-section and  $F(E_R)$  is nuclear form factor given by [36, 37]

$$\begin{aligned} F(E_R) &= \left[ \frac{3j_1(qR_1)}{qR_1} \right] \exp\left(\frac{q^2 s^2}{2}\right) \\ R_1 &= (r^2 - 5s^2)^{1/2} \\ r &= 1.2A^{1/3} \end{aligned} \quad (14)$$

where  $s$  ( $\simeq 1$  fm) is the thickness parameter of the nuclear surface,  $A$  is the mass number of the nucleus,  $j_1(qR_1)$  is the spherical Bessel function of index 1 and  $q = |\mathbf{q}| = \sqrt{2M_N E_R}$  as from Eq. (9). Assuming distribution  $f(v_{\text{gal}})$  of dark matter velocities ( $v_{\text{gal}}$ ) with respect to galactic rest frame to be Maxwellian, one can obtain the distribution  $f(v)$  of dark matter velocity ( $v$ ) with respect to earth rest frame by making the transformation

$$\mathbf{v} = \mathbf{v}_{\text{gal}} - \mathbf{v}_{\oplus} \quad (15)$$

where  $\mathbf{v}_{\oplus}$  is the velocity of earth with respect to Galactic rest frame and is given as a function of time  $t$  by

$$v_{\oplus} = v_{\odot} + v_{\text{orb}} \cos \gamma \cos\left(\frac{2\pi(t - t_0)}{T}\right) \quad (16)$$

In Eq. (16)  $v_{\odot}$  is the speed of the solar system in galactic rest frame,  $T$  (1 year) us the period of earth's rotation about sun ,  $t_0 = 2^{\text{nd}}$  June (the time of the year when the orbital velocity of earth and velocity of solar system point in the same direction) and  $\gamma \simeq 60^\circ$  is the angle subtended by earth orbital plane at Galactic plane. The speed of solar system  $v_{\odot}$  in the Galactic rest frame is given by

$$v_{\odot} = v_0 + v_{\text{pec}} \quad (17)$$

$v_0$  being the circular velocity of the local system at the position of solar system and  $v_{\text{pec}} = 12\text{km/sec}$ , called *peculiar velocity*, is speed of solar system with respect to the local system. Physical range of  $v_0$  is  $170 \text{ km/sec} \leq v_0 \leq 270 \text{ km/sec}$  (90 % C.L.) [38, 39]. In this work we consider the central value - 220 km/sec for  $v_0$ . The term  $\cos 2[\pi(t - t_0)/T]$  in the velocity is

responsible for annual modulation of dark matter signal. Introducing a dimensionless quantity  $T(E_R)$  as

$$T(E_R) = \frac{\sqrt{\pi}}{2} v_0 \int_{v_{\min}}^{\infty} \frac{f(v)}{v} dv \quad (18)$$

which can also be expressed as

$$T(E_R) = \frac{\sqrt{\pi}}{4v_{\oplus}} v_0 \left[ \operatorname{erf} \left( \frac{v_{\min} + v_{\oplus}}{v_0} \right) - \operatorname{erf} \left( \frac{v_{\min} - v_{\oplus}}{v_0} \right) \right] \quad (19)$$

we obtain from Eqs. (11) and (13)

$$\frac{dR}{dE_R} = \frac{\sigma^{\text{scalar}} \rho_s}{4v_{\oplus} M_S m_{\text{T}}^2} F^2(E_R) \left[ \operatorname{erf} \left( \frac{v_{\min} + v_{\oplus}}{v_0} \right) - \operatorname{erf} \left( \frac{v_{\min} - v_{\oplus}}{v_0} \right) \right] \quad (20)$$

The local dark matter density  $\rho_s$  may be taken as  $0.3 \text{ GeV/cm}^3$ . The observed recoil energy ( $E$ ) in the measured response of the detector is a fraction ( $Q_X$ ) of actual recoil energy ( $E_R$ ) at the time of scattering. This fraction  $Q_X = E/E_R$  (called as quenching factor) is different for different scattered nucleus  $X$ . For  $^{39}\text{Ar}$ ,  $Q_{\text{Ar}} = 0.76$ . Thus the differential rate in terms of the observed recoil energy  $E$  for  $^{39}\text{Ar}$  detector can be expressed as

$$\frac{\Delta R}{\Delta E}(E) = \int_{E/Q_{\text{Ar}}}^{(E+\Delta E)/Q_{\text{Ar}}} \frac{dR_{\text{Ar}}}{dE_R}(E_R) \frac{\Delta E_R}{\Delta E} \quad (21)$$

In left panel of Fig. 6 we show the expected differential rates (/kg/day/keV) for different observed recoil energies in Argon detector considering scalar singlet as the dark matter candidate. Four representative cases have been plotted and they are denoted as (a), (b), (c) and (d). For all the plots, (a) - (d), the chosen values of coupling  $\delta_2$  (as also corresponding scalar singlet masses,  $M_S$ ) are consistent with current CDMS and WMAP limits. All the plots show that the rate falls off with the increase of recoil energy. Plots (a) and (b) are the variations of rates for the same set of Higgs mass ( $M_h = 114 \text{ GeV}$ ) and singlet mass ( $M_S = 100 \text{ GeV}$ ) but for different values of the coupling  $\delta_2$  ( $\delta_2 = -0.1(-0.03)$  for plot (a) ((b)). Plots (a) and (b) show a decrease of the rate when  $|\delta_2|$  decreases. For example, in case of recoil energy  $E = 50 \text{ GeV}$  the calculated rates from plots (a) and (b) are  $8.5 \times 10^{-6}$  (for  $|\delta_2| = 0.1$ ) and  $7.2 \times 10^{-7}$  (for  $|\delta_2| = 0.03$ ) respectively in the units of /kg/day/keV. Plots (c) and (d) compare the variation of rates for two different scalar masses namely  $M_S = 200 \text{ GeV}$  (plot (c)) and  $M_S = 100 \text{ GeV}$  (plot (d)) for same values of  $M_h$ ,  $\delta_2$  ( $200 \text{ GeV}$ ,  $-0.03$ ). From plots (c) and (d) it is seen that the rate increases for any particular value of recoil energy with decrease of dark matter mass. For example in case of  $E = 50 \text{ GeV}$ , the rates for  $M_S = 100 \text{ GeV}$  (plot c) and  $M_S = 200 \text{ GeV}$  (plot d) the calculated rates are  $8 \times 10^{-8}$  and  $1.4 \times 10^{-8}$  respectively in the units of /kg/day/keV. This is evident from the expression for scalar cross section (Eq. (7) which varies as  $M_S^{-2}$  and direct detection rates is linear with the scalar cross section. One can compare plots (b) and (d) to see the effect of Higgs mass values on the rate. For  $M_S$ ,  $\delta_2$  ( $100 \text{ GeV}$ ,  $-0.03$ ), the estimated rates in the present calculations at  $E = 50 \text{ keV}$  are  $7.2 \times 10^{-7}$  (/kg/day/keV) for  $M_h = 114 \text{ GeV}$  (plot (b)) which is reduced to

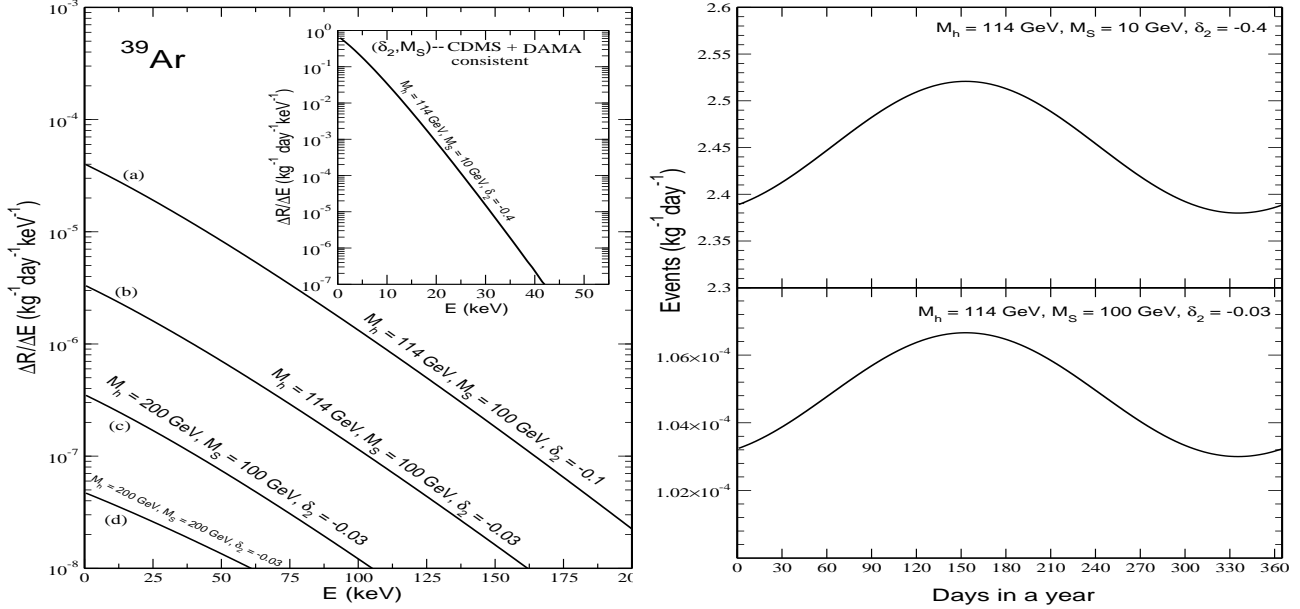


Figure 6: Left Panel: Plot of predictions for dark matter detection rates (per kg per day per keV) in Argon detector as a function of observed recoil energy. The plots are shown for two values of  $M_h$  - 114 GeV and 200 GeV and for two sets of  $(M_S, \delta_2)$  values which are consistent with CDMS limits as well as observed relic density of dark matter (WMAP). In the inset we show the corresponding plot for  $M_h = 114$  GeV and for two sets of  $(M_S, \delta_2)$  values simultaneously consistent with limits on scattering cross section from CDMS 2009 (GeV) and DAMA and also with WMAP. Right panel: Predicted annual variation of event rates in Argon detector over one year for  $M_h = 114$  (GeV). The upper panel corresponds to a  $(M_S, \delta_2)$  value consistent with CDMS+DAMA+WMAP while the lower panel corresponds to a  $(M_S, \delta_2)$  value consistent with CDMS+WMAP.

$1.4 \times 10^{-8}$  (/kg/day/keV) for  $M_h = 200$  GeV (plot (d)). In the inset of this same figure we show the calculated prediction of rates for  $M_S = 10$  GeV,  $\delta_2 = 0.4$ . This is compatible with the CDMS and DAMA bound together, other than satisfying the WMAP limits. The Higgs mass is kept at 114 GeV. As an example, for  $E = 30$  GeV the calculated expected event is  $1.4 \times 10^{-3}$  per day for a ton of the detector.

One very positive signature of dark matter in direct detection method is the annual variation of detection rate. This periodic variation arises due to periodic motion of the earth about the sun in which the directionality of earth's motion changes continually over the year. As a result, there is an annual variation in the amount of dark matter encountered by the earth. The detection of annual variation in direct detection experiments serve as a smoking gun signal for existence of dark matter. In right panel of Fig. 6 we show the calculated annual variation of event rate (/kg/day) in different times of a year. In the upper panel, we have chosen the parameter set that is compatible with CDMS, DAMA and WMAP limits (as in inset of the left panel) and for the lower panel we have given the results for  $M_h = 114$  GeV,  $M_S = 100$  GeV and  $\delta_2 = -0.03$ . As expected, the yield is maximum on 2nd June when the direction of motion of the earth is the

same as that of the solar system.

## 5 Summary and Conclusions

In the present work we consider a simplest extension of SM, introducing a real scalar singlet along with a discrete  $Z_2$  symmetry which ensures stability of the singlet. Such singlet is considered as a viable cold dark matter candidate. The scattering of this singlet dark matter off nuclei in the detector can be observed by measuring the energy of the recoil nuclei. The calculated singlet-nucleon scattering cross section in this model explicitly depends on the coupling  $\delta_2$  and implicitly on  $\kappa_2$  (as defined in Eq. (1)). We constrain the  $\delta_2 - \kappa_2$  parameter space using the recent bounds on the WIMP-nucleon scalar cross section as function of WIMP mass, reported by the CDMS collaboration and also reported by the XENON-10 and XENON-100 collaborations. The allowed zones in the parameter space follow a typical pattern determined by the shape of the WIMP mass dependence of the experimental limits considered here and the way the scalar singlet mass is related to  $\delta_2$  and  $\kappa_2$ . The allowed zones vary for different Higgs masses and they are consistent with WMAP limits.

We investigate the effect of the inclusion of DAMA results (with channelling) on the  $\delta_2 - \kappa_2$  parameter space but the allowed zone is found to be extremely small and representative of a very low dark matter mass (around  $\sim 10$  GeV). We also compute the range of  $\delta_2 - \kappa_2$  parameter space consistent with DAMA (without channelling) and CoGeNT experiments.

Utilising the constrained parameter space we estimate the possible detection rates and their annual variations for a liquid Argon detector.

**Acknowledgments:** We thank Probir Roy and Biswajit Adhikary for useful discussion. S.C. acknowledges support from the projects Centre for Astroparticle Physics and Frontiers of Theoretical Physics of Saha Institute of Nuclear Physics. A.G. and D.M. acknowledge the support from the DAE project ‘Investigating Neutrinoless Double Beta Decay, Dark Matter and GRB’ of Saha Institute of Nuclear Physics.

## References

- [1] D. E. McLaughlin, arXiv:astro-ph/9812242.
- [2] E. L. Lokas and G. A. Mamon, Mon. Not. Roy. Astron. Soc. **343**, 401 (2003) [arXiv:astro-ph/0302461].
- [3] M. Bradac, Nucl. Phys. Proc. Suppl. **194**, 17 (2009).
- [4] D. N. Spergel *et al.* [WMAP Collaboration], Astrophys. J. Suppl. **170**, 377 (2007); E. Komatsu *et al.* [WMAP Collaboration], Astrophys. J. Suppl. **180**, 330 (2009).
- [5] G. Jungman, M. Kamionkowski and K. Griest, Phys. Rept. **267**, 195 (1996) [arXiv:hep-ph/9506380].

- [6] K. Griest and M. Kamionkowski, Phys. Rept. **333**, 167 (2000).
- [7] G. Bertone, D. Hooper and J. Silk, Phys. Rept. **405**, 279 (2005) [arXiv:hep-ph/0404175].
- [8] H. Murayama, arXiv:0704.2276 [hep-ph].
- [9] J. McDonald, Phys. Rev. **D50**, 3637 (1994).
- [10] M. C. Bento, O. Bertolami, R. Rosenfeld and L. Teodoro, Phys. Rev. D **62**, 041302 (2000) [arXiv:astro-ph/0003350].
- [11] C. P. Burgess, M. Pospelov and T. ter Veldhuis, Nucl. Phys. B **619**, 709 (2001) [arXiv:hep-ph/0011335].
- [12] H. Davoudiasl, R. Kitano, T. Li, and H. Murayama, Phys. Lett. **B609**, 117 (2005), hep-ph/0405097.
- [13] R. Schabinger and J. D. Wells, Phys. Rev. D **72**, 093007 (2005) [arXiv:hep-ph/0509209].
- [14] D. O'Connell, M. J. Ramsey-Musolf, and M. B. Wise, (2006), hep-ph/0611014.
- [15] A. Kusenko, Phys. Rev. Lett. **97**, 241301 (2006) [arXiv:hep-ph/0609081].
- [16] O. Bahat-Treidel, Y. Grossman and Y. Rozen, JHEP **0705**, 022 (2007) [arXiv:hep-ph/0611162].
- [17] S. Andreas, arXiv:0905.0785 [hep-ph]
- [18] C. E. Yaguna, JCAP **0903**, 003 (2009) [arXiv:0810.4267 [hep-ph]].
- [19] X. G. He, T. Li, X. Q. Li, J. Tandean and H. C. Tsai, Phys. Lett. B **688**, 332 (2010) [arXiv:0912.4722 [hep-ph]].
- [20] S. Andreas, T. Hambye and M. H. G. Tytgat, JCAP **0810**, 034 (2008) [arXiv:0808.0255 [hep-ph]].
- [21] M. Cirelli and A. Strumia, New J. Phys. **11**, 105005 (2009) [arXiv:0903.3381 [hep-ph]].
- [22] O. Adriani *et al.* [PAMELA collaboration], Nature **458**, 607 (2009), O. Adriani *et al.*, Phys. Rev. Lett. **102**, 051101 (2009).
- [23] A. A. Abdo *et al.* [The Fermi LAT Collaboration], Phys. Rev. Lett. **102**, 181101 (2009) [arXiv:0905.0025 [astro-ph.HE]].
- [24] V. Barger, P. Langacker, M. McCaskey, M. J. Ramsey-Musolf and G. Shaughnessy, Phys. Rev. D **77**, 035005 (2008) [arXiv:0706.4311 [hep-ph]].
- [25] D. O'Connell, M. J. Ramsey-Musolf and M. B. Wise, Phys. Rev. D **75**, 037701 (2007) [arXiv:hep-ph/0611014].

- [26] Z. Ahmed *et al.* [The CDMS-II Collaboration], arXiv:0912.3592 [astro-ph.CO].
- [27] Z. Ahmed *et al.* (CDMS Collaboration), Phys. Rev. Lett. **103**, 141808 (2009); <http://ppd.fnal.gov/experiments/cdms/>
- [28] R. Bernabei *et al.* [DAMA collaboration], Eur. Phys. J. C **56**, 333 (2008); AIP Conf. Proc. **698**, 328 (2004); Int. J. Mod. Phys. D **13**, 2127 (2004).
- [29] J. Angle *et al.* (Xenon Collaboration), Phys. Rev. Lett. **100**, 021303 (2008), [arXiv:astro-ph/0706.0039]; E. Aprile and T. Doke, Rev. Mod. Phys. (2009).
- [30] E. Aprile (on behalf of Xenon collaboration) Proc. at TAUP 2009, J. Phys. Conf. Series **203**, 012005 (2010).
- [31] C. E. Aalseth *et al.* [CoGeNT collaboration], arXiv:1002.4703 [astro-ph.CO].
- [32] A. Rubbia, J. Phys.:Conference series **39** 129 (2006), TAUP 2005: Proc. Ninth Int. Conf. on Topics in Astroparticle and Underground Physics.
- [33] B. Beltran [for the PICASSO collaboration], J. Phys.:Conference series **136** 042080 (2008)
- [34] F. Petriello and K. M. Zurek, JHEP **0809**, 047 (2008) [arXiv:0806.3989 [hep-ph]].
- [35] N. Bozorgnia, G. B. Gelmini and P. Gondolo [arXiv:1006.3110 [astro-ph(CO)]]
- [36] R. H. Helm, Phys. Rev. **104**, 1466 (1956)
- [37] J. Engel, Phys. Lett. bf B264, 114 (1991)
- [38] P. J. T. Leonard and S. Tremaine, Astrophys. J. **353**, 486 (1990)
- [39] C. S. Kochanek, Astrophys. J. **457**, 228 (1996)